Author Manuscript

Author Manuscript

Author Manuscript

Author Manuscript

HHS Public Access

Author manuscript

Nat Mater. Author manuscript; available in PMC 2018 November 21.

Published in final edited form as:

Nat Mater. 2018 July ; 17(7): 642–651. doi:10.1038/s41563-018-0083-8.

Dual-function injectable angiogenic biomaterial for the repair of brain tissue following stroke

Lina R. Nih[1,2], **Shiva Gojgini**[1], **S. Thomas Carmichael**[2,*], and **Tatiana Segura**[1,3,*]

[1]Department of Chemical and Biomolecular Engineering, University of California, Los Angeles, USA

[2]Department of Neurology David Geffen School of Medicine, University of California, Los Angeles, USA

[3]Departments of Biomedical Engineering, Neurology, Dermatology Duke University 101 Science Drive, Durham NC 27707

Abstract

Stroke is the primary cause of disability due to the brain's limited ability to regenerate damaged tissue. After stroke, an increased inflammatory and immune response coupled with severely limited angiogenesis and neuronal growth results in a stroke cavity devoid of normal brain tissue. In the adult, therapeutic angiogenic materials have been used to repair ischemic tissues through the formation of vascular networks. However, whether a therapeutic angiogenic material can regenerate brain tissue and promote neural repair is poorly understood. Here we show that the delivery of an engineered immune-modulating angiogenic biomaterial material directly to the stroke cavity promotes tissue formation de novo, resulting in axonal networks along generated blood vessels. This regenerated tissue produces functional recovery through the established axonal networks. Thus, this biomaterials approach generates a vascularized network of regenerated functional neuronal connections within previously dead tissue, laying the groundwork for the use of angiogenic materials to repair other neurologically diseased tissues.

The lack of an effective medical therapy that promotes long-term recovery after stroke represents a substantial clinical burden, establishing a need for a medical treatment outside the confines of conventional therapies[1]. In the developing body, angiogenesis pioneers a vascular network that leads to the growth and maturation of the nervous system[2].

Users may view, print, copy, and download text and data-mine the content in such documents, for the purposes of academic research, subject always to the full Conditions of use: http://www.nature.com/authors/editorial_policies/license.html#terms

*Corresponding authors: Prof. Tatiana Segura, Tel.: +1-310-206-3980, tatiana.segura@duke.edu, Prof. Stanley Thomas Carmichael, Tel.: 310-206-9826, scarmichael@mednet.ucla.edu.

Author contributions

LRN was responsible for the conceptual design of the in vivo study, troubleshooting, experimental execution, interpretation of in vivo data, manuscript writing and figure creation. SG performed in vitro studies and interpretation, sample preparation and characterization, TS and STC contributed equally to overseeing experimental design and interpretation.

Competing interest

The authors claim no competing financial interests.

Data Availability Statement

The datasets generated and analysed during the current study are available from the corresponding author (tatiana.segura@duke.edu).

Author Manuscript Author Manuscript Author Manuscript Author Manuscript

Angiogenesis after stroke is associated with better outcomes in stroke patients[1] and promotes the formation of neurons through an endogenous neural stem cell response (post-stroke neurogenesis)[3, 4]. However, therapeutic manipulation of angiogenesis is problematic in the brain. The most dominant angiogenic growth factor, vascular endothelial growth factor (VEGF), is associated with an increase in blood brain barrier (BBB) opening, brain edema, and neurological deficits[5]. Other attempts at stimulating brain angiogenesis to promote recovery in stroke have also not been successful[6]. We sought to determine if a therapeutic angiogenic material, delivering an engineered presentation of VEGF directly to the stroke cavity, could stimulate angiogenesis and accompanying tissue repair after stroke.

Stroke causes tissue damage and the formation of a cavity. In this cavity, there is no extracellular matrix that supports cell infiltration into the lesion or to physically support a growing tissue[7]. Indeed, there is a glial barrier to cell entry[8]. Stroke also stimulates a massive local inflammatory response that may impede recovery[9]. Over time the cavity reorganizes into a fibrotic scar devoid of neural tissue[10]. Yet, the stroke cavity represents a potential transplant location because it can accept a large volume of injection without affecting normal brain[11, 12, 13, 14]. In addition, the delivery of therapies to the stroke cavity targets the area adjacent to stroke, the peri-infarct area, the site of the most robust neuronal and vascular plasticity after stroke[15]. A successful strategy for brain repair after stroke would deliver a molecule that stimulates angiogenesis and neural regeneration, reduces local inflammation, removes the barrier to cellular infiltration in the stroke site, and introduces a scaffold that can serve as a physical support onto which a neuronal network can grow. Recent advances in biopolymer hydrogels have developed materials with extracellular matrix motifs that directly support survival and cell infiltration[16, 17]. Given that the brain extracellular matrix is composed mostly of glycosaminoglycans and is devoid of fibrous extracellular matrix components[18], we chose to use an amorphous non-fibrous hydrogel composed of hyaluronic acid, which has been shown to promote neural differentiation[19], to serve as the backbone into which a VEGF delivery system would serve as the initial physical support for infiltrating cells, angiogenesis and axonogenesis. We have previously published a hydrogel-encapsulating soluble BDNF that aimed at promoting axonal ingrowth within the damaged site independently of a vascular route[20]. The results showed modest behavioral improvement and no tissue regeneration within the lesion site.

Injectable hydrogel for brain repair

An in situ gelling hyaluronic acid hydrogel (Supplementary Fig. 1, Supplementary Fig. 2a) that is both hyaluronidase degradable and MMP degradable (Supplementary Fig. 1, Supplementary Fig. 2a) was selected as the scaffold in which to build an artificial extracellular matrix to promote brain repair after stroke. Injection into the stoke cavity and in situ gelation 5 days after stroke did not significantly affect the cortex volume, size or shape compared to the contralateral side at 2-weeks post-stroke (Supplementary Fig. 3), indicating that the injection volume (6μL) and crosslinked hydrogel could be accommodated by the stroke cavity. Furthermore, injection of this hydrogel resulted in statistically decreased astrocyte activation (Supplementary Fig. 4) compared to a sham condition. However, this decrease in astrocyte scar thickness was not accompanied with an increase in brain repair as measured by angiogenesis, axonogenesis, and behavioral improvement, indicating that

Author Manuscript Author Manuscript Author Manuscript Author Manuscript

additional factors are required. We previously investigated slow VEGF release formulations (Supplementary Fig. 5) and shown that while there is an increase in vascularization and pericytes within the stroke cavity, this formulation did not result in improved neuronal tissue repair, indicating that in the context of stroke, sustained release of VEGF is not sufficient to promote neurological tissue repair.

Heparin nanoparticles alter the inflammatory and glial environment after stroke

We designed heparin nanoparticles so that they retained their ability to bind growth factors [21], including VEGF, but did not retain the native heparin ability to reduce blood coagulation (Supplementary Fig. 6). The dominant post-stroke inflammatory response of the brain is defined by the activation and recruitment to the damaged site of macrophages and microglia[9]. The initial extent of stroke damage correlates with intensity of microglia/macrophage activation in peri-infarct tissues[22]. HA gel + nH injection into the stroke cavity in distal MCAo significantly decreases microglial/macrophage levels (measured by IBA-1 – Ionized calcium-binding adapter molecule 1) as compared to empty gel or sham controls (Supplementary Fig. 4). The decrease in markers of inflammation was accompanied by a significantly increased vascularization within the stroke cavity and the peri-infact area (Fig. 1a–d, Fig. 2a,b,d) and an increase in immature neuron (DCX – Doublecortin positive) cell number (Fig. 3c). Recent evidence indicates that astrocyte activation in stroke and CNS lesions occurs in direct response to initial damage and restricts this damage[23, 24], providing a barometer of the evolving ischemic injury. nH significantly reduces the region of reactive astrocytes around the stroke cavity (Supplementary Fig. 4b). These gels do not modify the size of the stroke lesion itself (Supplementary Fig. 3d), suggesting that nH gel delivery to the stroke cavity reduces measures of long term damage in the tissue bordering the infarct. However, there was no difference of in-growth of axons within or around the stroke cavity in this condition.

VEGF clusters differentially activate endothelial cells

The HA gel was further engineered to promote angiogenesis. VEGF, bound to the extracellular matrix, signals through the clustering of VEGF receptors leading to sustained VEGF receptor-2 activation and altered downstream signaling compared to non-matrix bound VEGF[25]. Increasing ligand avidity through ligand clustering can enhance cellular activation, producing a more controlled tissue morphogenesis than with soluble factors[26]. Different clustering densities of VEGF were synthesized: low (lcV), medium (mcV) and high cluster (hcV, Supplementary Fig. 1, 2a–d). All VEGF clustering densities promoted the same level of endothelial cell proliferation (Supplementary Fig. 2e); however, VEGF receptor-2 (VEGFR-2) activation was significantly different between the different VEGF clustering densities. Y1175 and Y1214 in VEGFR-2 are major phosphorylation sites and we have previously shown differential activation upon presentation with bound or soluble VEGF[27]. These sites are also associated with the activation of the downstream signaling MAP kinases Erk1/2 (p42/44) and p38[28]. Phosphorylation at Y1175 and Y1214 by clustered VEGF displayed statistically higher phosphorylation for hcV than mcV or lcV

Author Manuscript Author Manuscript Author Manuscript Author Manuscript

(Supplementary Fig. 2f–h, $p < 0.05$) in response to a 5-min exposure to nH bound VEGF. There was no statistically significant difference between hcV and soluble VEGF (Vs) phosphorylation at Y1175 or Y1214. Interestingly, although no differences in downstream signal activation were observed for the different clustered VEGF presentations, there were differences when compared to Vs-induced activation: soluble VEGF preferentially activated p42/44, while clustered VEGF preferentially activated p38. The differences in downstream signal are reminiscent of what was observed for collagen bound and heparin bound VEGF versus soluble VEGF[29, 30, 31], indicating that VEGF bound to nH respond similarly to VEGF bound to bulk matrices.

hcV results in long-term revascularization of the stroke cavity

The brain tissue response to the angiogenic biomaterial (HA gel + hcV) was assessed after injection into the stroke cavity in distal MCAo 5-days post stroke (Supplementary Fig 1). Angiogenesis was measured at 2- and 16-weeks post stroke, representing a vessel maturation period and chronic period in tissue and behavioral recovery in stroke, respectively. At 2-weeks after stroke mice injected with HA gel containing the high clustered VEGF condition (HA gel + hcV) significantly increased endothelial cell area and proliferation (Glut-1 – Glucose transporter 1) and pericyte (PDGFR-β – Platelet-derived growth factor receptor-β) area in and around the stroke cavity (Fig. 1a–f) compared to HA gel containing the low VEGF cluster (lcV), nanoparticles only (nH), soluble VEGF (Vs) or HA gel only. Heparin nanoparticle-only group also outperformed every other group but was significantly lower than the hcV condition hcV. Since VEGF delivery to the brain has previously been associated with immature vessels, lacking pericyte coverage[32], we tested whether endothelial and pericyte markers were colocalized. We found that HA gel + hcV stimulated vascular structures with pericyte coverage (Fig. 1f). In addition, the quantification of Angiopoietin-2, known to play a distinct role in angiogenesis and in coupling of angiogenesis to other elements of tissue repair[33], showed a significant increase in the peri-infarct area in the hcV brain compared with the No gel and gel + Vs conditions, in the close vicinity of vessels (Supplementary Fig. 7).

Therapeutic angiogenic materials often have a short-term angiogenic response that subsides and vessels regress as the angiogenic stimulus (e.g. VEGF) is depleted[34]. HA gel + hcV resulted in a significantly increased vascular area inside the stroke cavity while no significant difference between groups was observed in the peri-infarct area (Fig. 2a,b). Inside the infarct, the increased angiogenesis led to a vascular area greater than the contralateral side, indicating a vascular network that is more substantial than the original network in this cortical area. After stroke, the normal process of angiogenesis leads to a tortuous and dilated vasculature[31]. We assessed the vascular tortuosity, branching points, vessel diameter and infiltration distance within the infarct cavity of the induced vessels[35] compared to normal vessels in the contralateral side at the 16-week time point. HA gel + hcV showed a lower degree and variability of vessel tortuosity and was closer to the tortuosity of normal vessels (Fig. 2c(1). There was no significant difference in the number of vascular ramifications between groups (Fig. 2d(1). Finally, the stroke cavity with HA gel + hcV displayed a significantly reduced vascular diameter compared with HA gel + soluble VEGF (Fig. 2c(2), with a value close to the contralateral normal control side and a

Author Manuscript Author Manuscript Author Manuscript Author Manuscript

significantly greater vascular infiltration distance into the lesion site compared with any other group (Fig. 2d(2).

Interestingly, while no effect on blood-brain barrier (BBB) permeability was observed at the 2-week time point (Supplementary Fig. 4), a significantly increased infarct size was found in the Vs condition (Supplementary Fig. 3), consistent with previous reports that soluble VEGF administration in stroke may worsen stroke outcome[36]. This increased stroke volume observed in the Vs condition 2 weeks after stroke is maintained at 16 weeks post-stroke (Supplementary Fig. 8).

Revascularization of the stroke cavity leads to neurogenesis and axonogenesis

We tested the hypothesis that by promoting a dense and well-formed vascular bed inside the stroke cavity, the development of an accompanying neural structure would follow. Neurogenesis after stroke occurs to a limited degree as neuroblasts migrate from their origin in the subventricular zone to areas of damage. Neurogenesis in the present experiments was assessed by staining neuroblasts (Dcx) 10-days or 16 weeks after gel transplantation in distal MCAo stroke. The number of proliferative neuroblasts (Dcx/BrdU - Bromodeoxyuridine) was significantly increased in the hcV compared with the No gel control group (Fig. 3c). The total number of Dcx cells in the SVZ was also significantly increased in both the HA gel + hcV and HA gel + nH conditions compared with any other group. Similarly, these two conditions display a significantly increased number of Dcx cells along the corpus callosum, the migratory path towards the lesion, compared with any other group, with no significant difference in the migrating distance (Fig. 3d). These results may be due to the increased angiogenic signal in HA gel + hcV and HA gel + nH conditions (Fig. 1d), or due to reductions in tissue barriers at this site. The addition of VEGF did not change the inflammatory response to HA gel + nH, which continued to have significantly reduced the microglial positive area and astrocytic scar thickness compared with mice injected with low cluster VEGF (Gel + lcV), soluble VEGF (Gel + Vs), Empty gel and No gel control 2 weeks after stroke (Supplementary Fig. 4, 8). This early increase in immature neurons in the peri-infarct cortex was not sustained: at 16 weeks there were no significant differences between groups in the number of Dcx cells (Supplementary Fig. 9). This data suggests that the presence of naked heparin particles found in both gel + nH and gel + hcV conditions induces migration of immature neuroblasts into the damaged tissue adjacent to the stroke cavity at initial stages during tissue recovery after stroke.

We next determined if angiogenesis could promote the infiltration of axons into the stroke lesion site as it does in the normal body during development[37]. Three separate assessments were performed to assess axonogenesis at 2- and 16-weeks utilizing a marker for axons, neurofilaments (NF200 – Neurofilament 200) and assessing its density in the infarct and peri-infarct areas, neurofilament infiltration distance, and neurofilament infiltration angle (a measure of the orientation of the axonal network). At both 2 weeks (Fig. 3e,f) and 16 weeks after stroke (Fig. 3h–j), only the hcV had significantly more neurofilament area compared with the other conditions. These axons had a significantly deeper axonal infiltration distance

Author Manuscript Author Manuscript Author Manuscript Author Manuscript

into the infarct, and a penetrating angle that is similar to the angle measured between the NF200 axons and the cortex in the contralateral side (Fig. 3k) which suggests that the formed axonal network in the hcV condition is a structured in a similar linear pattern to the normal cortical axonal network. Interestingly at 16 weeks the NF200 positive area in the high cluster VEGF condition is higher than the contralateral value (dotted line) in the homologous cortex that is not affected by stroke (Fig. 3h,i) indicating that similar to the formed vasculature in the hcV-treated brains, the axonal ingrowth into the stroke cavity establishes a network of connections that is greater than the underlying brain structure of cortex.

To further study the connection of the vascular network with the formed axonal network, we co-stained vessels (Glut-1) and neurofilament networks (NF200) at 16-weeks. We found a very close association between the vessels and neurofilaments in the hcV brains (Fig. 4a,b) with a statistically higher percent of neurofilaments that are either in direct contact with (Fig. 4c) or within 50μm of a vessel (Fig. 4d), further confirming the role of vessels in forming a reparative neurovascular niche that leads to axonogenesis within the stroke cavity.

To prove that the observed axonogenesis was due to the revascularization of the stroke cavity and not a direct effect of VEGF on sprouting neurons[38, 39], we blocked angiogenesis through a VEGF independent mechanism using endostatin during days 5 to 15 after stroke and analyzed the neurofilament network at 16 weeks. This approach blocks angiogenesis in this stroke-hydrogel-VEGF approach[40]. We found a significant reduction of the vascular area (Supplementary Fig. 10a), growth (Supplementary Fig. 10b) and infiltration (Supplementary Fig. 10c) of endostatin-injected HA + hcV mice at 16 weeks post-stroke. The blockade of angiogenesis in HA gel + hcV mice is associated with a statistical reduction of the axonal network area in and around the stroke (Fig. 4a,b), particularly in the vicinity of vessels (Fig. 4c), indicating that angiogenesis is causally linked to the axonogenesis observed in the hcV condition. These results show that inducing angiogenesis into the infarct can generate an elaborate neuronal architecture within this normally fibrotic cavity. In order to identify the neuronal population that sends axonal projections to the stroke site of gel + hcV –treated mice, we delivered BDA (biotinylated dextran amine), a marker for bidirectional axonal tracing in the gel injection coordinates on Week 16 after gel treatment (Fig. 4d). BDA uptake was visualized fluorescently using a streptavidin-fluorochrome detection. Brain sections were co-stained with the astrocytic marker GFAP – Glial fibrillary acidic protein (in order to visualize the site of lesion. We found that neurons sending axonal projections in the injected cavity of hcV mice are located in the in the ipsilateral peri-infarct cortex, with a clear detection of retrogradely traced cell bodies up to 800μm distant from the site of injection.

Last, we aimed to determine whether the formed vasculature in the gel + hcV brains present characteristics of functional maturity with both coverage with pericytes (PDGFR-β, Fig. 4e) and astrocytic endfeet (Aquaporin-4, Fig. 4f). Fluorescent staining shows a strong vascular coverage with both pericytes and end-feet astrocytes, associated with GFAP-expressing astrocyte cell bodies in the vicinity of vessels, further indicating that in this condition, normal brain architecture is achieved.

Author Manuscript Author Manuscript Author Manuscript Author Manuscript

From a therapeutic angiogenic material to a functional axonal network

In order to test whether the induced vascular and neuronal tissue in the stroke cavity is associated with functional recovery, behavioral recovery was measured after hydrogel transplantation. Photothrombotic stroke in the forelimb motor cortex causes limb use deficits in mice for at least 16 weeks after the infarct[41]. Mice received this stroke and were transplanted 5 days later with HA gel, HA gel + Vs, HA gel + lcV and HA gel + hcV (Fig. 5a). Limb control was measured with 3 different behavioral tests every 4 weeks for 16 weeks, in order to assess the dexterity of the contralateral forelimb (Cylinder test/asymmetry score, Fig. 5b(1), hindlimb (Grid test/footfault, Fig. 5b(2) and forepaw (Pasta test/paw adjustment and time in seconds, Fig. 5b(3–4) in measures that reflect human motor control patterns after stroke[42]. Stroke causes a deficit in limb motor control in exploratory rearing, gait and dexterous forepaw use that is maximal at 4 and 8 weeks after the infarct with some recovery but still a persistent deficit at 12 and 16 weeks. HA gel + hcV-injected animals displayed a significantly increased use of their contralateral forelimb in exploratory rearing in the cylinder task beginning 12 weeks after stroke (Fig. 5b(1), and a significant decrease in the number of contralateral footfaults on the grid walk task at the same point (Fig. 5b(2). The pasta handling test showed the HA gel + hcV condition produced a significantly reduced time to manipulate and eat a piece of pasta on weeks 8 to 16 (Fig. 5b(3), while showing a significantly increased use of contralateral digits in handling the pieces of food (Fig. 5b(4). No other gel or VEGF condition was associated with this degree of enhanced functional recovery. These results indicate a dramatic decrease in limb use deficits for high cluster VEGF condition, suggesting that the axonal network observed in HA + hcV delivery is functionally active.

To prove that the observed functional recovery was linked to angiogenesis due to the formed axonal network in the stroke cavity, we performed two separate tests. First, we used endostatin to block angiogenesis as previously done (Supplementary Fig. 10). Since blocking angiogenesis significantly reduced neurofilament density and infiltration distance (Fig. 3g–j), blocking angiogenesis should also prevent the functional improvement observed if the formed axonal network or vascular network are responsible for the observed improvement. Treatment with endostatin impaired the recovery observed in the high cluster VEGF condition, showing a significantly decelerated recovery compared with the HA gel + hcV animals, and this in all the behavioral tasks performed (Fig. 5c(1–4), demonstrating that VEGF induced angiogenesis is critical in the observed functional recovery. To test if the enhanced functional recovery in the HA + hcV condition was due to the axonal connections observed in the infarct (Fig. 5d(1–4), we retrogradely transfected the neurons that extend these axons into the infarct (Fig. 4a,d) by injecting an AAV construct that expresses a neuronal silencing receptor, hM4D DREADD[43] directly into the infarct site. Neurons that form connections into the damaged tissue and the HA gel + hcV gel will be inhibited when CNO, the ligand for hM4D, is administered. This technique has been used to silence neuronal activity in a specific area of rodent brain[43]. At week 13, a time period of enhanced motor recovery in HA gel + hcV, neurons that project into the hcV gel were silenced with CNO (Fig. 5a). Initially, HA gel + hcV treated stroke animals showed enhanced functional recovery, replicating the earlier results of this gel. However, when these animals were treated

Author Manuscript Author Manuscript Author Manuscript Author Manuscript

with CNO, the improved motor functions were lost and the animal deficit was worsened (Fig. 5d(1–4), demonstrating that the formed axonal network is responsible for the observed functional improvement. In total, these studies indicate HA gel + hcV promotes development of a neurovascular brain tissue within a normally fibrotic scar and promotes functional recovery through angiogenesis and stimulated axonal ingrowth into a network of connections from adjacent brain.

Naked heparin particles are essential for the pro-repair properties of hcV

The injected high and low cluster treatments (respectively hcV and lcV) were designed to contain equal amounts of heparin and VEGF (Supplementary Fig. 1). Though we showed that heparin particles have a reduced blood thinning ability compared to polymeric heparin (Fig. 6, Supplementary Fig. 11), the introduction of naked heparin particles to the hcV group complicates clinical translation. Thus, we wanted to determine if the delivery of high cluster VEGF alone would perform similarly as high cluster VEGF + heparin nanoparticles. We injected mice with gels containing only heparin particles coated with VEGF at high cluster density and removed the unloaded naked particles (hcV-nH). The results showed that similarly to the hcV treatment, the hcV-nH treatment enhanced post-stroke angiogenesis at 2 weeks (Fig. 6a,b). This pro-angiogenic effect was maintained in the peri-infarct 16 weeks after stroke (Supplementary Fig 11a,b). However, the increase in angiogenesis was accompanied with an increase in inflammation (Fig. 6a,c), characteristic of VEGF delivery in brain and other organ systems[44]. Both microglia area and glial scar thickness were significantly increased in the hcV-nH condition compared with hcV, showing an inflammation worse than in the empty gel control group (Fig. 6e). Further, no axonal growth was observed in this group (Fig. 6d). The pro-inflammatory effect of the hcV – nH was also observed at 16 weeks, where the microglia area and the scar thickness was maintained significantly higher than in hcV (Supplementary Fig 11c,e).

The results obtained with the hcV-nH conditions show that axonal formation that follows therapeutic angiogenesis requires immune-modulation of injury-induced inflammation. The absence of post-stroke immune-modulation results in vasculature that is not followed by tissue repair. Similarly, we tested whether the addition of naked heparin particles to lcV, a VEGF cluster group that did not show pro-repair effect in the brain, would increase its beneficial effects. This experimental condition, lcV + nH, was tested for the same repair characteristics at 2 (Fig. 6) and 16 weeks (Supplementary Fig. 11). The results show that the lcV + nH treatment did not promote vascular (Fig. 6b) or axonal growth (Fig. 6d), did not reduce the microglial inflammation (Fig. 6C) or the scar thickness (Fig. 6e) 2 weeks after stroke. The same results were observed at 16 weeks post-stroke (Supplementary Fig 11a–d). The results obtained with lcV + nH show that the combination of VEGF and naked particles is not enough to promote brain repair, as the therapeutic effect of heparin particles is only observed with high VEGF clusters.

To investigate the effect of heparin nanoparticles on inflammatory and anti-inflammatory cytokine levels after stroke, a multiplex ELISA was performed. Mice were stroked and injected with gel + nH five days post stroke. Three and 10 days after gel transplantation, the infarct core with the injected gel were harvested and quantified for their levels of cytokines

Author Manuscript Author Manuscript Author Manuscript Author Manuscript

(TNF-α, IL-6, IFN-γ, IL-1 α, IL-1 β, IL-2, IL-4 and IL-10). We found that gel + nH significantly decreased brain concentration of TNF-α 3 days after the gel injection (P =0.0076). At this time point, gel + nH does not show any significant difference with the No stroke condition (Supplementary Fig. 12, Supplementary notes 2).

Conclusion

The stroke cavity is a fibrotic region devoid of neurons and with a sparse, disordered vasculature. The cavity represents the tissue lost after stroke and is associated with functional disability in stroke patients. This report shows that engineering a VEGF-containing hydrogel biomaterial and injecting it directly within the stroke cavity induces the formation of a vascular and neuronal structure that leads to behavioral improvement. The HA gel + hcV induce the formation of a robust, mature and highly developed vascular bed within the stroke cavity and patterned axonal ingrowth along these vessels. This vascular bed is mature as compared to the normal vascular structure in cortex in its morphology and pericyte coverage. This is unexpected in a traditional delivery of VEGF in the brain[32] and indicates that the clustered nanoparticle presentation of VEGF in the hydrogel promotes elements of normal vascular development. This distinctive vascular development in hydrogel-presented nanoparticle-clustered VEGF is supported by the differential VEGFR2 phosphorylation and downstream p38 signaling of clustered VEGF. This hydrogel also modifies the adjacent peri-infarct tissue, by reducing microglia activation, the size of the reactive astrocyte border and by promoting in-migration of immature neurons from the subventricular zone. HA + hcV hydrogels promote vascular in-growth into the infarct cavity and an accompanying axonal network. These formed axons inside the stroke cavity are tightly physically associated with the generated vascular network, and selective blockade of vascular in-growth blocks the development of this axonal network inside the cavity. These findings support a process of coordinated vascular and axonal growth in a developing neural tissue inside a normally fibrotic brain scar. In the developing body, and particularly in skin, development of the vascular and neuronal networks are tightly coordinated through shared molecular signaling systems, such as Slits, semaphorins, netrins and VEGF[45]. In the present study, co-delivery of nanoparticle-clustered VEGF and heparin nanoparticles were sufficient to induce this ingrowth and co-patterning of vascular and neuronal systems, but is likely to have done so by initiating a process that may be locally sustained by these other signaling systems.

Although the anti-coagulant properties of heparin are well established, increasing evidence indicates that heparin presents many anti-inflammatory effects linked to its ability to block leucocyte adhesion to the vessel wall[46] and to stabilize chemokine and growth factor gradients[47], but also act as a reservoir of heparin binding cytokines[48]. Here, we hypothesize that the immuno-modulation properties of naked particles result from its ability to bind and decrease brain levels of stroke-induced pro-inflammatory cytokine TNF-α directly at the lesion site. Moreover, the high inflammation found in lcV, where all heparin particles are bound to VEGF, further indicates that the anti-inflammatory properties of heparin particles are exclusively observed in their un-bound state. VEGF delivery has been associated with increased inflammation, which lowers efficacy and increases adverse effects[44]. Here we show that naked heparin particles, can counter balance the inflammatory effect of VEGF and

Author Manuscript Author Manuscript Author Manuscript Author Manuscript

lead to the formation of a pro-repair environment that leads to brain tissue formation de novo.

Injection of a hydrogel into the stroke cavity has been tested in large animal stroke models[20], and provides a tractable way to approach the post-infarct brain without damaging or manipulating viable tissues around the infarct, which are a site of substantial repair[15]. This combination of direct production of a neurovascular structure in the infarct cavity and modulation of inflammatory, scar and neural stem cells responses in the adjacent brain position this approach as unique in the field of neural repair.

Materials and Methods

Heparin nanoparticle synthesis and VEGF binding

Heparin (from porcine intestinal mucosa, Alfa Aesar) was modified with p-azidobenzyl hydrazide (ABH) as previously described[49]. The remaining carboxylic acid groups on heparin were then conjugated with N-(3-Aminopropyl) methacrylamide in 27 molar excess through EDC coupling chemistry overnight in PBS buffer, dialyzed against distilled (DI) water, and lyophilized. The final product was dissolved in a 100 mg/ml solution of sodium acetate at pH 4, mixed with Tween-80 and Span-80 (8% HLB) and sonicated to form nanoparticles. A radical polymerization was initiated as previously described [49]. A total concentration of 20μg/ml VEGF (Genentech, Telbermin) was mixed with concentrations of heparin nanoparticles ranging from 0.1 to 0.001 mg/mL to form different packing densities of VEGF onto the particle's surface, incubated overnight and exposed to UV light (365 nm) for 10 minutes to covalently bind VEGF to heparin particles. The VEGF nanoparticles were washed from excess with 0.05% Tween-20, then with PBS, using a 100 kD MWCO dialysis units. The washes were collected and an Elisa and Dot blot were performed to estimate the amount of VEGF bound to nanoparticles by subtracting the washes to the total amount of VEGF mixed.

Heparin nanoparticle characterization

Dynamic Light Scattering (DLS) was used to characterize the Z-average (diameter) and polydispersity index (PDI) of heparin nanoparticles after each preparation step. Samples were analyzed by a Malvern Zetasizer where ten runs of three measurements each were performed. In order to confirm the results obatiend by DLS, Transmission Electron Microscopy (TEM) with a T12 Quick CryoEM was performed on heparin particles (1 mg/mL) using a carbon-coated copper grid (300 mesh). The nanoparticles were negatively stained by 2 wt % photungstic acid (PTA) solution.

Enzyme linked immunosorbant assay (ELISA) and Dot Blot

The amount of VEGF immobilized onto nanoparticles in the different clustering conditions was measured using a standard ELISA technique as previously described[50]. A Dot blot was also realized in order to confirm the Elisa results: a 2μl drop of the sample was deposited on a nitrocellulose membrane. A blocking buffer of BSA (1% in PBS) was used before adding the biotinylated detection antibody, followed by streptavidin-HRP. The samples were then visualized using chemifluorescence (ECL detection reagents, GE Healthcare) using a

Author Manuscript Author Manuscript Author Manuscript Author Manuscript

Molecular Imager Chemi Doc XRS+ scanner (Bio Rad). The stained membrane images were analyzed with Image Lab software.

VEGFR-2 phosphorylation assay

Human Umbilical Vein Endothelial Cells (HUVECs, LONZA, CC-2519) were cultured as previously described[29].

RNA Isolation and Real Time q-PCR

HUVECs were grown up to 70% confluency in complete EGM media (Lonza, Switzerland). Cells were submitted to serum depravation for 5 h., before exposing them to fetal bovine serum basal EGM-2 media at different time points (2, 4, 6 h). Cells were trypsinized and the cell pellet was collected. Lysis buffer from the RNAqueous micro total RNA isolation kit (Ambion, Life Technologies) was immediately added to cell pellet. RNA concentration was evaluated by UV absorbance (λ = 260 nm). Reverse transcription was carried out by loading 0.25 μg RNA per reaction of the iScript Advanced cDNA synthesis kit (Bio-Rad). Quantitative real-time PCR (qPCR) was carried out using 10 ng cDNA per reaction of the Maxima SYBR Green/ROX qPCR master mix (Thermo Scientific, Pittsburgh, PA, USA) following the manufacturer's recommended protocol for three-step cycling using the StepOnePlus real-time PCR system (Applied Biosystems, Life Technologies). Every 20-μl reaction contained 5μl of cDNA, 12.5 μl SYBR Green master mixes (life technology), 250 nM forward, reverse primers, and nuclease free water. Threshold cycles (CT) were evaluated by the bundled software and expression fold change was calculated using the delta-delta CT method assuming 100% efficiency. GAPDH was used as the housekeeping gene.

Proliferation assay

Proliferation rate of HUVEC cells exposed to different clusters of VEGF was evaluated using a Cell Proliferation Assay Kit (CyQUANT®, Invitrogen). Briefly, cells were grown in complete EGM-2 media in a 96 well-plate for 2–4 hrs for cell attachment and exposed to VEGF nanoparticle of different cluster density, in basal EBM media with 2% fetal bovine serum (Lonza, Basal, Switzerland) and compared to a negative control condition containing no VEGF. After 2 days of culture, cells were lysed and the relative fluorescence was measured at 485 nm excitation and 528 nm emissions. The data are expressed as relative fluorescence to a condition where cells were exposed to only heparin particles only.

Tail vein bleeding assay

C57BL/6 male mice of 8–12 weeks (Jackson Laboratories) were put under isoflurane anesthesia (2–2.5% in a 70% N2O/30% O2 mixture), then placed on a warming pad and injected intravenously with heparin, heparin particles or saline (4 U/kg, 50 μl). Thirty minutes later, the lateral vein was incised transversally over a position corresponding to a diameter of 2.5 mm. The tail is then immersed in warm PBS (37°C) in a conical tube until the vein stops bleeding (tail vein bleeding time, in seconds).

Author Manuscript Author Manuscript Author Manuscript Author Manuscript

Hyaluronic acid modification and hydrogel gelation

Hyaluronic acid (60,000 Da, Genzyme, Cambridge, MA) was functionalized as previously described[13].

Gelation

The hydrogel was made as previously described[53]. We have previously found that clustered bioactive signals such as the adhesion peptide RGD results in significant differences in cell behaviour when encapsulated inside three-dimensional HA [53]. The highest degree of cell spreading, integrin expression and proliferation of encapsulated mouse mesenchymal stem cells was obtained with a ratio of 1.17 mole of RGD-reacting HA for 1 mole of RGD. The RGD peptide was dissolved in 0.3 M HEPES and added to 16% of the total HA-AC required to obtain a degree of clustering of 1.17, and reacted for 20 minutes at room temperature before being added to the rest of non-RGD reacting HA-AC. A total of 200 ng of soluble (Gel + Vs) or heparin nanoparticle-bound VEGF 165 (Gel + hcV, Gel + lcV) was added to the gel precursor solution.

Animal experiment design

Animal procedures were performed in accordance with the US National Institutes of Health Animal Protection Guidelines and approved by the Chancellor's Animal Research Committee as well as the UCLA Office of Environment Health and Safety. C57BL/6 male mice of 8–12 weeks (Jackson Laboratories), were used in the study. Two stroke models were performed: A permanent and distal Middle cerebral artery occlusion (MCAo) and photo-thrombotic (PT). The MCAo model closely simulates human ischemic stroke and its peri-infarct penumbra[54] as approximately 70% of human infarcts originate from the MCA. In addition, this model is considered suitable for the study of ischemia-induced cell death, inflammation, and blood–brain barrier (BBB) damage in the brain, and has therefore been used in the majority of studies that address post-stroke repair mechanisms such as neurogenesis and angiogenesis[55]. This model was chosen for the 2 week time point in order to evaluate the effect of the gel + hcV treatment on vascularization. However, because the permanent and distal MCAo model doesn't induce a long-term neurological deficit, the PT model was used to assess the neurological deficit for 16 weeks.

Middle Cerebral Artery Occlusion (MCAO) stroke model

MCAo model was induced under 2% anesthesia by exposing and occluding by electrocoagulation the anterior branch of the distal left MCA through a craniotomy over the parietal cortex. The MCAo-induced ischemic cellular damage is localized on the somatosensory and motor cortex[56] and was chosen because of the high re-vascularization process after stroke in this region[57, 58].

Photothrombotic (PT) stroke model

The PT stroke was induced using a intraperitoneally-injected light-sensitive dye as previously described[59]. Briefly, mice were positioned in a stereotaxic instrument and administered Rose Bengal (10 mg/ml, i.p.) and the closed skull at the stereotaxic coordinate 1.5 mm medial/lateral was illuminated with a white light for 18 minutes.

Author Manuscript Author Manuscript Author Manuscript Author Manuscript

Hydrogel and VEGF intracranial transplantation

Five days following stroke surgery, 6 μL of RGD – functionalized HA hydrogel containing the different forms of VEGF was injected directly into the stroke cavity through a 30-gauge needle attached to a 25 μL Hamilton syringe (Hamilton, Reno, NV). A syringe pump maintained the infusion rate at 1 μL/min in the following coordinates anterior-posterior (AP) = 0.26 mm, medial-lateral [60] = 3 mm, and dorso-ventral (DV) = 1 mm and 1.5 mm for MCAo and PT mice, respectively. Control group were injected with an empty RGD-functionalized gel (Empty gel). This time point for VEGF injection was selected according to published literature on on the time frame of VEGF up-regulation in the stroke brain and the peak of peri-infarct microvascular density[61]. Ten days following hydrogel transplantation, animals were injected intraperitoneally with the 5-bromo-2′-deoxyuridine (BrdU, Sigma, St Louis, MO) at a concentration of 100 mg/kg, 4 and 2 hours before euthanasia to assess cell proliferation.

Mouse tissue processing and immunohistochemistry

At 2 weeks post-stroke (10 days after transplantation), mice were transcardially perfused with 40 mL of 4% (wt/vol) paraformaldehyde (PFA). Brains were harvested and post-fixed in 4% PFA overnight and immersed in 30% sucrose for 2 days for cryoprotection. Tangential sectioning of frozen brains (30 μm-thick) were obtained using a cryostat and placed on gelatin-coated glass slides. Immunohistochemistry includes washing steps using PBS and permeabilization/blockage using Triton (0.3%) and Normal Donkey Serum (10%). Primary antibodies were as follows: Rabbit anti-Glucose Transporter 1 (Glut-1-) (1:200; Abcam, Cambridge, MA) for vascular Endothelial Cells; goat anti- Platelet-derived Growth Factor Receptor β (1:400; PDGF-Rβ, R&D Systems, Minneapolis, MN) for pericytes; goat anti-doublecortin (DCX) (C18, 1:500; Santa Cruz Biotechnology, Santa Cruz, CA) for subventricular neural progenitor cells; rat anti-BrdU (1:300; Abcam, Cambridge, MA); rat anti-GFAP (1:400; Zymed, San Francisco, CA) for astrocytes; rabbit anti-microglial-specific ionized calcium binding adaptor molecule 1 (Iba-1) (1:250; Wako Pure Chemical Industries, Japan) for microglial cells; rabbit anti-Neurofilament 200 (NF200) (1:100; Sigma-Aldrich, St Louis, MO), mouse anti-Angiopoietin-2 (1:100; Abcam, Cambridge, MA), rabbit anti-Aquaporin-4 (1:250; Abcam, Cambridge, MA). Primary antibodies were incubated overnight at +4°C followed by fluorescently labeled secondary antibody (1:1000; Jackson Imuno-research, West Grove, PA, USA) for 1 h at room temperature. Cell nuclei were labeled using DAPI (4′, 6-diamidino-2-phenylindole, (DAPI, 1:2000, Invitrogen) for 10 minutes, followed by a step of dehydration in ethanol, and dewaxing in xylene. For BrdU staining, sections were incubated with 2N HCl and sodium borate buffer (pH 8.4) before addition of the primary antibody[62].

Microscopy and Morphoanalysis

Analyses were performed as previously described[63]. The scar thickness was measured on the ischemic boundary zone within the ipsilateral hemisphere on 3 sections stained for GFAP. The NF200 infiltration within the ischemic core represents the average of the length of axonal sprouts penetrating in the infarct area. The Dcx migration was measured on the

Author Manuscript Author Manuscript Author Manuscript Author Manuscript

ipsilateral hemisphere and represents the length of migration of Dcx positive neuroblasts along the Corpus Callosum.

Assessment of Infarct, hemispheres and cortex volume

Quantification of infarct, ipsilateral and contralateral hemispheres and cortex was performed using a upright Leica DMLB microscope (Microbrightfield hardware and software, Williston, VT, USA). For each animal, every 10th coronal sections were stained for NeuN and Dapi and digitized using Stereo Investigator (Microbrightfield). The volumes were calculated by combining the measured areas with the section thickness. All values obtained were averaged and represented as one single value per animal.

Evaluation of Blood-Brain Barrier (BBB) permeability

BBB permeability was evaluated as previously described [40]. The absorbance of the solution was measured at 625 nm. A ratio absorbance ipsilateral/contralateral was obtained and expressed as unit/g dry weight as previously described[64].

Endostatin treatment

Endostatin (Recombinant mouse, 100 μg/ml; Alpha Diagnostic, San Antonio, TX), a VEGF-independent angiogenesis inhibitor, was injected subcutaneously daily during days 5–15 after stroke to hcV-treated mice. hcV-Endostatin mice were submitted to behavioral tests and their brain used for immunohistology at 16 weeks time point.

AAV5 brain injection

An additional set of hcV-injected mice were injected at week 13 after stroke with a viral construct AAV5 construct expressing hM4 DREADD receptors (designer receptors exclusively activated by a designer drug), capable of silencing transfected neurons after attachment to an i.p administered drug clozapine-N-oxide (CNO) on week 16. A total volume of 1 μL of AAV5 was injected in the stroke site at an infusion rate of 0.1 μL/min. The AAV5 vector as a tool to study the direct association between brain activity in the infarcted zone and the behavioral outcome. Indeed, the CNO/DREAAD system was shown to inhibit the action potential (AP) of transfected cells through the activation of Inwardly Rectifying K+ channels, provoking a massive entrance of K+ ions and a subsequent hyperpolarization of the cell [65]. Thus the administration of CNO inhibits the neurotransmitter transport within the injected site, here the infarcted area, 30 minutes after injection and remains active for a period of 2 hours without compromising cells integrity. A behavioral test was then be performed within the AP silent window, to assess whether hcV-induced axons in the stroke site participate to the behavioral outcome.

BDA brain injection

A total volume of 1 μL of BDA (biotinylated dextran amine), an efficient and powerful marker for bidirectional axonal tracing, was injected in the stroke site at an infusion rate of 0.1 μL/min, in gel + hcV –treated mice, 16 weeks after stroke. Mice were sacrificed 5 days later and BDA staining was visualized fluorescently by immunohistology using a one-step streptavidin-fluorochrome detection.

Author Manuscript Author Manuscript Author Manuscript Author Manuscript

Cytokine analysis

Animals were stroked and injected with gel + nH five days later. The contralateral brain at 10-days (no stroke) and stroke only served as positive and negative controls, respectively. At 3 and 10 days after gel transplantation, animals were placed under anesthesia and perfused intracardially with PBS to flush out blood. Harvested brains were dissected and the infarct core with the injected gel were dissected and homogenized. A total of 1.5 mg/mL of sample was then diluted 1:1 with PBS+ 0.5% fetal bovine serum and quantified for their levels of cytokines using a multiplex Elisa analysis through the Bio-Plex kit (Bio-rad Laboratories Inc.) for the following cytokines: TNF-α, IL-6, IFN-γ, IL-1 α, IL-1 β, IL-2, IL-4 and IL-10.

Behavioral deficit assessment

The cylinder test / spontaneous forelimb task and the Grid-walking test were performed as previously described[59]. For the pasta test, mice were submitted to food restriction 1 day prior to the test, then placed in a cylinder and were given a total number of 4 pieces of uncooked vermicelli (7 cm length, 1.5 mm diameter; De Cecco Capellini), once piece at a time and videotaped while eating. A total of 3 criterias were quantified: 1) number of adjustments (release-regrasp) per forepaw per piece of pasta. 2) The time to eat one piece of pasta (in secondes). 3) Atypical pasta handling behaviors as previously described[41].

Statistics

Statistical analyses were performed as previously described [63] for both histology (minimum n=5) and behavioral tests (n=12). For endostatin –related analysis, two-tailed unpaired test was used for the comparison of two groups (hcV and hcV + endostatin). The results are expressed as mean ± SEM. Single, double, triple and quadruple asterisks represent $P < 0.05$, $P < 0.01$, $P < 0.001$ and $P < 0.0001$, respectively. A P value < 0.05 was considered statistically significant. The BDA axonal tracing, histology for vascular coverage at 16 weeks and characterization of heparin particles by TEM were repeated independently three times with similar results.

Supplementary Material

Refer to Web version on PubMed Central for supplementary material.

Acknowledgments

This work was supported through the US National Institutes of Health NIH RO1NS079691. The Bioplex experiment was done at the UCLA IMT core, Center for Systems Biomedicine, which is supported by CURE/P30 DK041301.

References

1. Go AS, Mozaffarian D, Roger VL, Benjamin EJ, Berry JD, Blaha MJ, et al. Heart disease and stroke statistics--2014 update: a report from the American Heart Association. Circulation. 2014; 129(3):e28–e292. [PubMed: 24352519]
2. Larrivee B, Freitas C, Suchting S, Brunet I, Eichmann A. Guidance of vascular development: lessons from the nervous system. Circ Res. 2009; 104(4):428–441. [PubMed: 19246687]
3. Ohab JJ, Fleming S, Blesch A, Carmichael ST. A neurovascular niche for neurogenesis after stroke. J Neurosci. 2006; 26(50):13007–13016. [PubMed: 17167090]

Author Manuscript Author Manuscript Author Manuscript Author Manuscript

4. Lindvall O, Kokaia Z. Neurogenesis following Stroke Affecting the Adult Brain. Csh Perspect Biol. 2015; 7(11)
5. Zhang ZG, Zhang L, Jiang Q, Zhang R, Davies K, Powers C, et al. VEGF enhances angiogenesis and promotes blood-brain barrier leakage in the ischemic brain. The Journal of clinical investigation. 2000; 106(7):829–838. [PubMed: 11018070]
6. Ergul A, Alhusban A, Fagan SC. Angiogenesis: a harmonized target for recovery after stroke. Stroke. 2012; 43(8):2270–2274. [PubMed: 22618382]
7. Huang L, Wu ZB, Zhuge Q, Zheng W, Shao B, Wang B, et al. Glial scar formation occurs in the human brain after ischemic stroke. International journal of medical sciences. 2014; 11(4):344–348. [PubMed: 24578611]
8. Sofroniew MV, Vinters HV. Astrocytes: biology and pathology. Acta Neuropathol. 2010; 119(1):7–35. [PubMed: 20012068]
9. Dirnagl U, Iadecola C, Moskowitz MA. Pathobiology of ischaemic stroke: an integrated view. Trends Neurosci. 1999; 22(9):391–397. [PubMed: 10441299]
10. Fitch MT, Doller C, Combs CK, Landreth GE, Silver J. Cellular and molecular mechanisms of glial scarring and progressive cavitation: in vivo and in vitro analysis of inflammation-induced secondary injury after CNS trauma. J Neurosci. 1999; 19(19):8182–8198. [PubMed: 10493720]
11. Nih LR, Carmichael ST, Segura T. Hydrogels for brain repair after stroke: an emerging treatment option. Current opinion in biotechnology. 2016; 40:155–163. [PubMed: 27162093]
12. Nih LR, Moshayedi P, Llorente IL, Berg AR, Cinkornpumin J, Lowry WE, et al. Engineered HA hydrogel for stem cell transplantation in the brain: Biocompatibility data using a design of experiment approach. Data in brief. 2017; 10:202–209. [PubMed: 27995155]
13. Moshayedi P, Nih LR, Llorente IL, Berg AR, Cinkornpumin J, Lowry WE, et al. Systematic optimization of an engineered hydrogel allows for selective control of human neural stem cell survival and differentiation after transplantation in the stroke brain. Biomaterials. 2016; 105:145–155. [PubMed: 27521617]
14. Zhu S, Nih LR, Carmichael ST, Lu Y, Segura T. Enzyme-Responsive Delivery of Multiple Proteins with Spatiotemporal Control. Adv Mater. 2015; 27(24):3620–3625. [PubMed: 25962336]
15. Carmichael ST. Cellular and molecular mechanisms of neural repair after stroke: making waves. Ann Neurol. 2006; 59(5):735–742. [PubMed: 16634041]
16. Chai C, Leong KW. Biomaterials approach to expand and direct differentiation of stem cells. Mol Ther. 2007; 15(3):467–480. [PubMed: 17264853]
17. Orive G, Anitua E, Pedraz JL, Emerich DF. Biomaterials for promoting brain protection, repair and regeneration. Nature reviews Neuroscience. 2009; 10(9):682–692. [PubMed: 19654582]
18. Lau LW, Cua R, Keough MB, Haylock-Jacobs S, Yong VW. Pathophysiology of the brain extracellular matrix: a new target for remyelination. Nat Rev Neurosci. 2013; 14(10):722–729. [PubMed: 23985834]
19. Hou S, Xu Q, Tian W, Cui F, Cai Q, Ma J, et al. The repair of brain lesion by implantation of hyaluronic acid hydrogels modified with laminin. Journal of neuroscience methods. 2005; 148(1): 60–70. [PubMed: 15978668]
20. Cook DJ, Nguyen C, Chun HN, ILL, Chiu AS, Machnicki M, et al. Hydrogel-delivered brain-derived neurotrophic factor promotes tissue repair and recovery after stroke. J Cereb Blood Flow Metab. 2017; 37(3):1030–1045. [PubMed: 27174996]
21. Fairbrother WJ, Champe MA, Christinger HW, Keyt BA, Starovasnik MA. Solution structure of the heparin-binding domain of vascular endothelial growth factor. Structure. 1998; 6(5):637–648. [PubMed: 9634701]
22. Walter HL, Walberer M, Rueger MA, Backes H, Wiedermann D, Hoehn M, et al. In vivo analysis of neuroinflammation in the late chronic phase after experimental stroke. Neuroscience. 2015; 292:71–80. [PubMed: 25701708]
23. Anderson MA, Burda JE, Ren Y, Ao Y, O'Shea TM, Kawaguchi R, et al. Astrocyte scar formation aids central nervous system axon regeneration. Nature. 2016; 532(7598):195–200. [PubMed: 27027288]

Author Manuscript Author Manuscript Author Manuscript Author Manuscript

24. Chen ZL, Yao Y, Norris EH, Kruyer A, Jno-Charles O, Akhmerov A, et al. Ablation of astrocytic laminin impairs vascular smooth muscle cell function and leads to hemorrhagic stroke. J Cell Biol. 2013; 202(2):381–395. [PubMed: 23857767]
25. Ferrara N, Gerber HP, LeCouter J. The biology of VEGF and its receptors. Nature Medicine. 2003; 9(6):669–676.
26. Conway A, Vazin T, Spelke DP, Rode NA, Healy KE, Kane RS, et al. Multivalent ligands control stem cell behaviour in vitro and in vivo. Nat Nanotechnol. 2013; 8(11):831–838. [PubMed: 24141540]
27. Lee KW, Yoon JJ, Lee JH, Kim SY, Jung HJ, Kim SJ, et al. Sustained release of vascular endothelial growth factor from calcium-induced alginate hydrogels reinforced by heparin and chitosan. Transplant Proc. 2004; 36(8):2464–2465. [PubMed: 15561282]
28. Chung C, Burdick JA. Influence of Three-Dimensional Hyaluronic Acid Microenvironments on Mesenchymal Stem Cell Chondrogenesis. Tissue Engineering Part A. 2009; 15(2):243–254. [PubMed: 19193129]
29. Anderson SM, Shergill B, Barry ZT, Manousiouthakis E, Chen TT, Botvinick E, et al. VEGF internalization is not required for VEGFR-2 phosphorylation in bioengineered surfaces with covalently linked VEGF. Integrative biology : quantitative biosciences from nano to macro. 2011; 3(9):887–896. [PubMed: 21826315]
30. Lee S, Jilani SM, Nikolova GV, Carpizo D, Iruela-Arispe ML. Processing of VEGF-A by matrix metalloproteinases regulates bioavailability and vascular patterning in tumors. J Cell Biol. 2005; 169(4):681–691. [PubMed: 15911882]
31. Wei L, Erinjeri JP, Rovainen CM, Woolsey TA. Collateral growth and angiogenesis around cortical stroke. Stroke. 2001; 32(9):2179–2184. [PubMed: 11546914]
32. Ma Y, Zechariah A, Qu Y, Hermann DM. Effects of vascular endothelial growth factor in ischemic stroke. J Neurosci Res. 2012; 90(10):1873–1882. [PubMed: 22714747]
33. Eklund L, Olsen BR. Tie receptors and their angiopoietin ligands are context-dependent regulators of vascular remodeling. Exp Cell Res. 2006; 312(5):630–641. [PubMed: 16225862]
34. Bramfeldt H, Sabra G, Centis V, Vermette P. Scaffold vascularization: a challenge for three-dimensional tissue engineering. Current medicinal chemistry. 2010; 17(33):3944–3967. [PubMed: 20939827]
35. Lorthois S, Lauwers F, Cassot F. Tortuosity and other vessel attributes for arterioles and venules of the human cerebral cortex. Microvasc Res. 2014; 91:99–109. [PubMed: 24291593]
36. Arai K, Jin G, Navaratna D, Lo EH. Brain angiogenesis in developmental and pathological processes: neurovascular injury and angiogenic recovery after stroke. Febs J. 2009; 276(17):4644–4652. [PubMed: 19664070]
37. Adams RH, Eichmann A. Axon guidance molecules in vascular patterning. Cold Spring Harb Perspect Biol. 2010; 2(5):a001875. [PubMed: 20452960]
38. Barami K. Relationship of neural stem cells with their vascular niche: implications in the malignant progression of gliomas. J Clin Neurosci. 2008; 15(11):1193–1197. [PubMed: 18617407]
39. Ruiz de Almodovar C, Fabre PJ, Knevels E, Coulon C, Segura I, Haddick PC, et al. VEGF mediates commissural axon chemoattraction through its receptor Flk1. Neuron. 2011; 70(5):966–978. [PubMed: 21658588]
40. Nih LR, Deroide N, Lere-Dean C, Lerouet D, Soustrat M, Levy BI, et al. Neuroblast survival depends on mature vascular network formation after mouse stroke: role of endothelial and smooth muscle progenitor cell co-administration. Eur J Neurosci. 2012; 35(8):1208–1217. [PubMed: 22512253]
41. Allred RP, Adkins DL, Woodlee MT, Husbands LC, Maldonado MA, Kane JR, et al. The vermicelli handling test: a simple quantitative measure of dexterous forepaw function in rats. J Neurosci Methods. 2008; 170(2):229–244. [PubMed: 18325597]
42. Li S, Nie EH, Yin Y, Benowitz LI, Tung S, Vinters HV, et al. GDF10 is a signal for axonal sprouting and functional recovery after stroke. Nat Neurosci. 2015; 18(12):1737–1745. [PubMed: 26502261]
43. Smith KS, Bucci DJ, Luikart BW, Mahler SV. DREADDS: Use and application in behavioral neuroscience. Behavioral neuroscience. 2016; 130(2):137–155. [PubMed: 26913540]

Author Manuscript Author Manuscript Author Manuscript Author Manuscript

44. Croll SD, Ransohoff RM, Cai N, Zhang Q, Martin FJ, Wei T, et al. VEGF-mediated inflammation precedes angiogenesis in adult brain. Exp Neurol. 2004; 187(2):388–402. [PubMed: 15144865]
45. Busse CE, Krotkova A, Eichmann K. The TCRbeta enhancer is dispensable for the expression of rearranged TCRbeta genes in thymic DN2/DN3 populations but not at later stages. J Immunol. 2005; 175(5):3067–3074. [PubMed: 16116195]
46. Wan MX, Zhang XW, Torkvist L, Thorlacius H. Low molecular weight heparin inhibits tumor necrosis factor alpha-induced leukocyte rolling. Inflamm Res. 2001; 50(12):581–584. [PubMed: 11822782]
47. Handel TM, Johnson Z, Crown SE, Lau EK, Proudfoot AE. Regulation of protein function by glycosaminoglycans--as exemplified by chemokines. Annual review of biochemistry. 2005; 74:385–410.
48. Lohmann N, Schirmer L, Atallah P, Wandel E, Ferrer RA, Werner C, et al. Glycosaminoglycan-based hydrogels capture inflammatory chemokines and rescue defective wound healing in mice. Sci Transl Med. 2017; 9(386)
49. Anderson SM, Siegman SN, Segura T. The effect of vascular endothelial growth factor (VEGF) presentation within fibrin matrices on endothelial cell branching. Biomaterials. 2011; 32(30): 7432–7443. [PubMed: 21783250]
50. Anderson SM, Chen TT, Iruela-Arispe ML, Segura T. The phosphorylation of vascular endothelial growth factor receptor-2 (VEGFR-2) by engineered surfaces with electrostatically or covalently immobilized VEGF. Biomaterials. 2009; 30(27):4618–4628. [PubMed: 19540581]
51. Lei Y, Gojgini S, Lam J, Segura T. The spreading, migration and proliferation of mouse mesenchymal stem cells cultured inside hyaluronic acid hydrogels. Biomaterials. 2011
52. Zhu J, Marchant RE. Design properties of hydrogel tissue-engineering scaffolds. Expert review of medical devices. 2011; 8(5):607–626. [PubMed: 22026626]
53. Lam J, Lowry WE, Carmichael ST, Segura T. Delivery of iPS-NPCs to the Stroke Cavity within a Hyaluronic Acid Matrix Promotes the Differentiation of Transplanted Cells. Adv Funct Mater. 2014; 24(44):7053–7062. [PubMed: 26213530]
54. Liu S, Zhen G, Meloni BP, Campbell K, Winn HR. Rodent Stroke Model Guidelines for Preclinical Stroke Trials (1st Edition). Journal of experimental stroke & translational medicine. 2009; 2(2):2–27. [PubMed: 20369026]
55. Fluri F, Schuhmann MK, Kleinschnitz C. Animal models of ischemic stroke and their application in clinical research. Drug design, development and therapy. 2015; 9:3445–3454.
56. Carmichael ST. Rodent models of focal stroke: size, mechanism, and purpose. NeuroRx : the journal of the American Society for Experimental NeuroTherapeutics. 2005; 2(3):396–409. [PubMed: 16389304]
57. Carmichael ST. Emergent properties of neural repair: elemental biology to therapeutic concepts. Ann Neurol. 2016; 79(6):895–906. [PubMed: 27043816]
58. Carmichael ST. The 3 Rs of Stroke Biology: Radial, Relayed, and Regenerative. Neurotherapeutics : the journal of the American Society for Experimental NeuroTherapeutics. 2016; 13(2):348–359. [PubMed: 26602550]
59. Clarkson AN, Huang BS, Macisaac SE, Mody I, Carmichael ST. Reducing excessive GABA-mediated tonic inhibition promotes functional recovery after stroke. Nature. 2010; 468(7321):305–309. [PubMed: 21048709]
60. Scott AK, Gregory HR, Kevin JG, Armando M, Joel PF, Clifford RJ, et al. Magnetic resonance elastography of the brain. NeuroImage. 2008; 39(1):231–237. [PubMed: 17913514]
61. Salhia B, Angelov L, Roncari L, Wu X, Shannon P, Guha A. Expression of vascular endothelial growth factor by reactive astrocytes and associated neoangiogenesis. Brain Res. 2000; 883(1):87–97. [PubMed: 11063991]
62. Tsai PT, Ohab JJ, Kertesz N, Groszer M, Matter C, Gao J, et al. A critical role of erythropoietin receptor in neurogenesis and post-stroke recovery. J Neurosci. 2006; 26(4):1269–1274. [PubMed: 16436614]
63. Li S, Nih LR, Bachman H, Fei P, Li Y, Nam E, et al. Hydrogels with precisely controlled integrin activation dictate vascular patterning and permeability. Nature materials. 2017

Author Manuscript Author Manuscript Author Manuscript Author Manuscript

64. Fukui S, Fazzina G, Amorini AM, Dunbar JG, Marmarou A. Differential effects of atrial natriuretic peptide on the brain water and sodium after experimental cortical contusion in the rat. J Cereb Blood Flow Metab. 2003; 23(10):1212–1218. [PubMed: 14526231]

65. Rogan SC, Roth BL. Remote control of neuronal signaling. Pharmacological reviews. 2011; 63(2): 291–315. [PubMed: 21415127]

66. Schallert T, Fleming SM, Leasure JL, Tillerson JL, Bland ST. CNS plasticity and assessment of forelimb sensorimotor outcome in unilateral rat models of stroke, cortical ablation, parkinsonism and spinal cord injury. Neuropharmacology. 2000; 39(5):777–787. [PubMed: 10699444]

Author Manuscript Author Manuscript Author Manuscript Author Manuscript

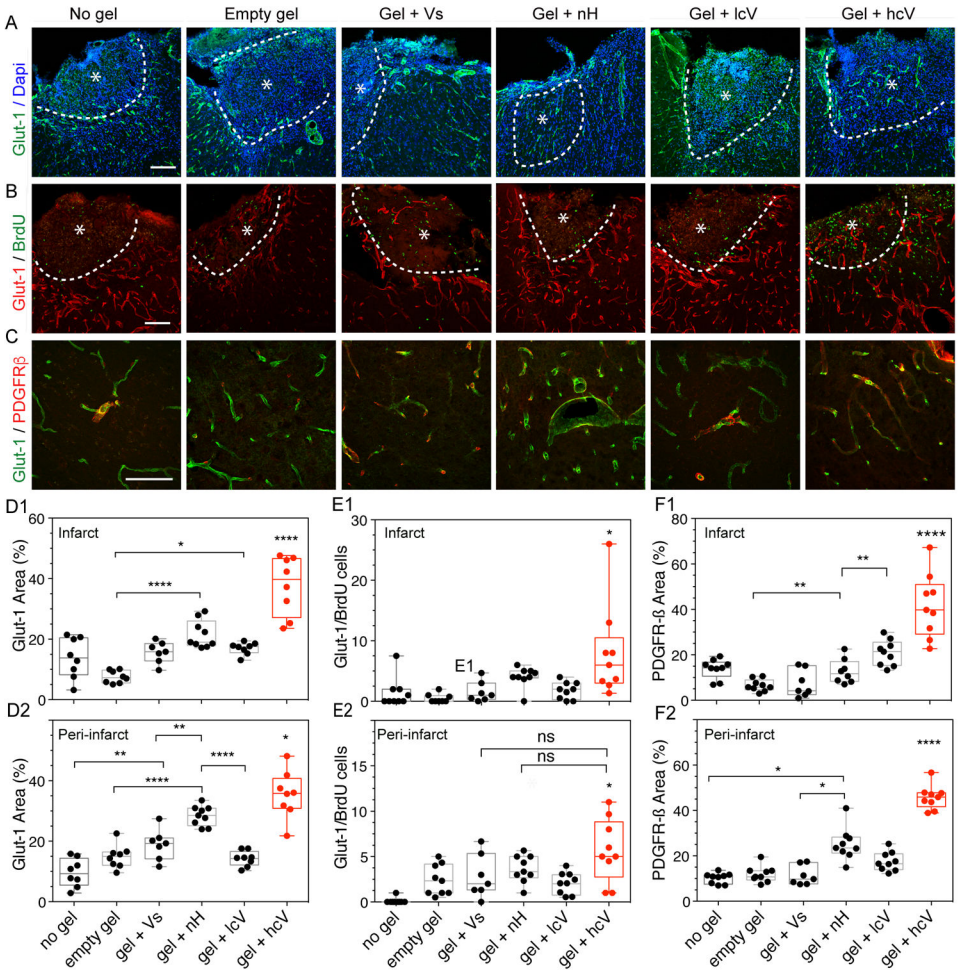

Figure 1. Post-stroke angiogenic response and vascular remodeling

(A) Fluorescent images of vessels (Glut-1) with Dapi, (B) a marker of proliferation (BrdU), and (C) pericyte/smooth muscle cells (PDGFR-β) in and around the stroke site (*) at day 10 after gel transplantation. Quantification of the vascular density (% Glut-1 area) in the infarct (D1) and peri-infarct (D2), angiogenesis (Glut-1/BrdU cells) in the infarct (E1) and peri-infarct (E2) and pericyte vascular coverage (% PDGFR-β area) in the infarct (F1) and peri-infarct area (F2). No gel = stroke only condition, empty gel = HA hydrogel, gel + Vs = HA hydrogel loaded with 200ng of soluble VEGF, gel + nH = HA hydrogel with 1μg heparin nanoparticles (nH), gel + lcV = HA hydrogel with 1μg nH loaded with 200 ng VEGF, gel + hcV = HA hydrogel with 0.01 μg nH loaded with VEGF and 0.99 μg unloaded nH. Data is presented using a min to max box plot. Each dot in the plots represents one animal and p values were determined by One-way ANOVA with a Tukey's post-hoc test, with *, ** and **** indicating $p < 0.05$, $p < 0.01$ and $p < 0.0001$, respectively. Scale bar: 100 μm.

Author Manuscript Author Manuscript Author Manuscript Author Manuscript

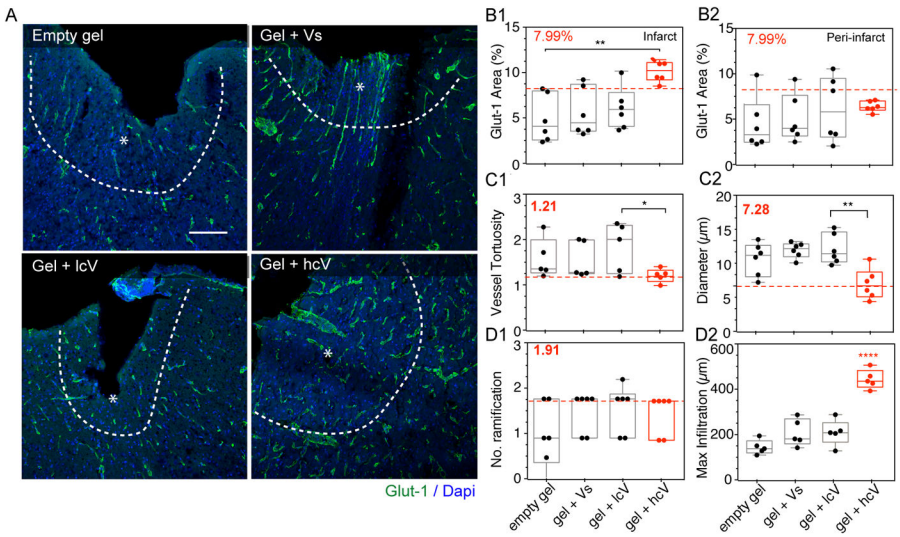

Figure 2. Long-term post-stroke vascular growth

(A) Fluorescent images of vessels (Glut-1) in and around the stroke site (*) 16 weeks after gel transplantation. (B) Quantification of the vascular density (% Glut-1 area) in and around the stroke site (*), Quantification of the vessel morphology: vessel tortuosity = total vessel length/shortest distance (C1) and diameter (C2), Quantification of vessel growth with number of ramifications = the number of branches/vessel (D1) and maximum infiltration distance of the vessels into the stroke site (D2). In all plots, the dotted red line and red number indicates the value for the give quantification of the contralateral side. Empty gel = gel = HA hydrogel, Vs = 200 ng of soluble VEGF, lcV = 1μg nH loaded with 200 ng VEGF, hcV = 0.01 μg nH loaded with VEGF and 0.99 μg unloaded nH. Data is presented using a min to max box plot. Each dot in the plots represents one animal and p values were determined by One-way ANOVA with a Tukey's post-hoc test, with *, ** and **** indicating $p < 0.05$, $p < 0.01$ and $p < 0.0001$, respectively. Scale bar: 100 μm.

Author Manuscript Author Manuscript Author Manuscript Author Manuscript

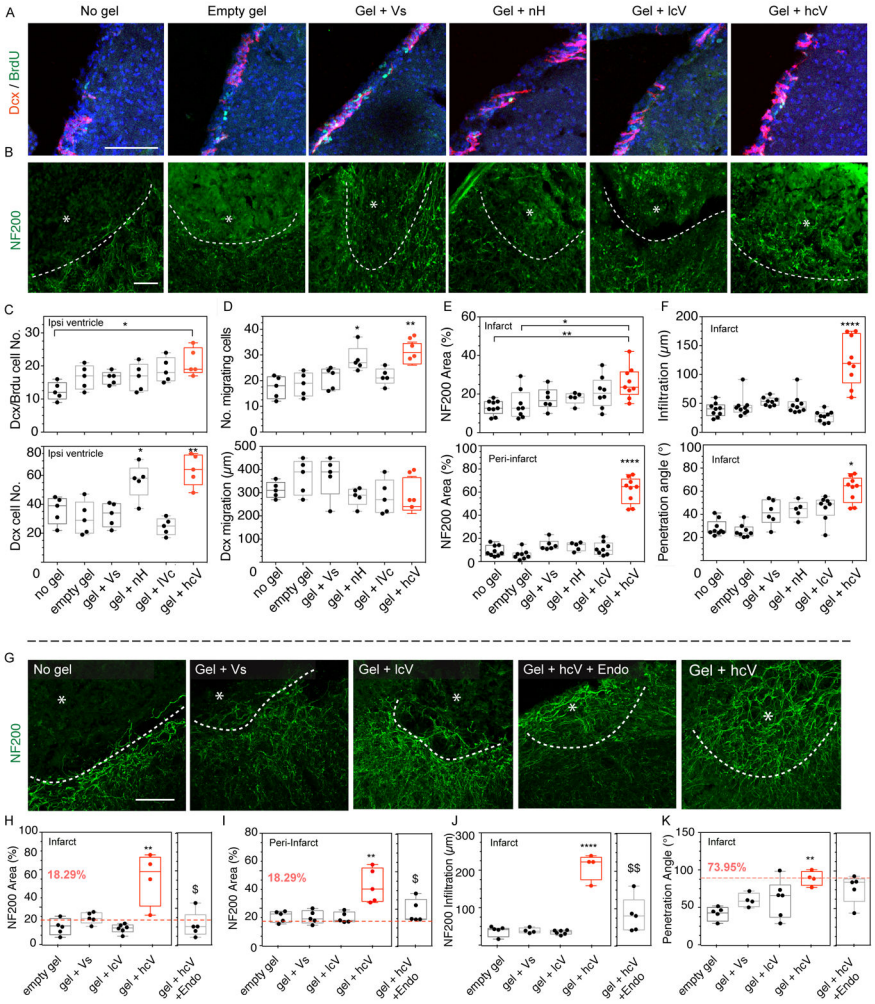

Figure 3. Post-stroke neurogenesis and axonal sprouting

(A) Fluorescent images of neuroblasts (Dcx) and the proliferation marker BrdU, and (B) axonal neurofilaments (NF200) in and around the stroke site (*) at 2 weeks and (G) at 16 weeks after gel transplantation. (C) Quantification of neuroblasts (Dcx) and proliferating neuroblasts (Dcx/BrdU) in the ipsilateral ventricle, (D) the number of neuroblasts migrating and their migration distance and number, (E) the axonal area (NF200) in and around the stroke site, and (F) infiltration distance and penetration angle in the stroke site. (H) Quantification of axonal area (NF200) in and (I) around the stroke site, (J) infiltration distance and (K) axonal penetration angle 16 weeks after gel injection. In all plots, the dotted red line and red number indicates the value for the give quantification of the contralateral side. Empty gel = gel = HA hydrogel, Vs = 200 ng of soluble VEGF, lcV = 1μg nH loaded with 200 ng VEGF, hcV = 0.01 μg nH loaded with 200 ng VEGF and 0.99 μg unloaded nH, Endo = a daily i.p injection of endostatin day 5 to 15. Data is presented using a min to max box plot. Each dot in the plots represents one animal and p values were determined by One-way ANOVA with a Tukey's post-hoc test, with *, ** and **** indicating $p < 0.05$, $p < 0.01$ and $p < 0.0001$, respectively. Scale bar: 100 μm.

Author Manuscript Author Manuscript Author Manuscript Author Manuscript

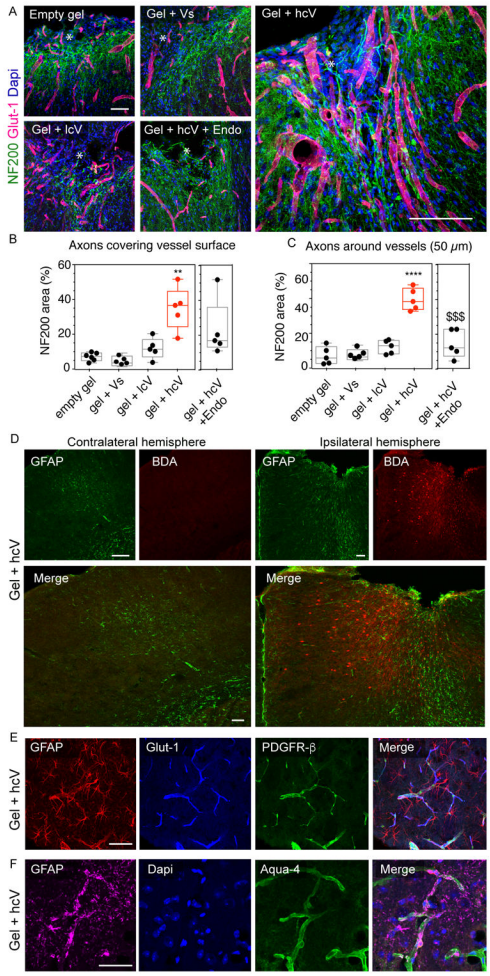

Figure 4. Association between the vascular and axonal network in the lesion site

(A) Fluorescent images of vessels (Glut-1, red) and axonal neurofilaments (NF200, green) in and around the stroke site (*) 16 weeks after gel transplantation. (B) Quantitative assessment of the proximity between the 2 networks with the quantification of NF200 positive signal on vessels and (C) positive area a distance of 50 μm from vessels. (D) Fluorescent images of the peri-infarct astrocytic scar (GFAP, green) and BDA-traced neurons (red) in the ipsilateral hemisphere of gel + hcV injected mice 16 weeks after gel transplantation. (E) Fluorescent images of astrocytes (GFAP) co-stained with vessels (Glut-1) and pericytes/smooth muscle cells (PDGFR-β), or (F) with end-feet astrocytes (Aquaporin-4) in the stroke site of hcV-treated mice, 16 weeks after gel transplantation. Empty gel = gel = HA hydrogel, Vs = 200 ng of soluble VEGF, lcV = 1μg nH loaded with 200 ng VEGF, hcV = 0.01 μg nH loaded with 200 ng VEGF and 0.99 μg unloaded nH, Endo = a daily i.p injection of endostatin days 5 to 15. Data is presented using a min to max box plot. Each dot in the plots represents one animal and p values were determined by One-way ANOVA with a Tukey's post-hoc test, with ** and **** indicating $p < 0.01$ and $p < 0.0001$, respectively. Data represent the average. $$$ indicates $p < 0.001$ vs Gel+hcV. Scale bar: 100 μm.

Author Manuscript Author Manuscript Author Manuscript Author Manuscript

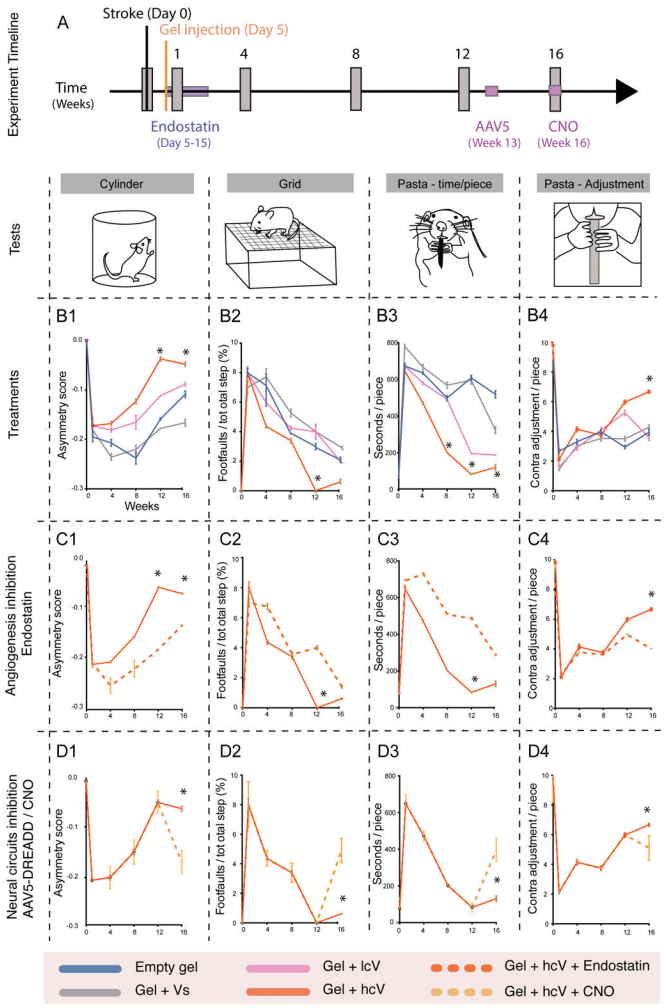

Figure 5. Post-stroke neurological recovery

(A) Experiment timeline for the behavioral tests. Mice were injected 5 days after stroke with one of the following treatments: empty gel, gel + Vs, gel + lcV, and gel + hcV. Mice were subjected to different behavioral tests (illustrated by vertical grey boxes on the timeline) On week 0, 1, 4, 8, 12 and 16 after stroke. (B1) The Cylinder test was used to measure the dexterity of their contralateral forelimb, (B2) the Grid test for the contralateral hindlimb, and (B3, B4) the Pasta test for the contralateral forepaw, normally sensitive to post-stroke lateralized impairments. (C1–C4) In order to determine the role of gel+hcV -induced vascularization on behavioral recovery, a supplemental set of gel+hcV animals was administered with endostatin, a VEGF-independent angiogenic inhibitor for 10 days after the gel injection, and submitted to the same behavioral tests: Cylinder (C1), Grid (C2), and Pasta (C3–C4). (D1–D4) In order to determine the role of gel+hcV –induced axonal growth on recovery, a supplemental set of gel+hcV animals received a brain injection of an AAV5 viral construct expressing hM4 DREADD receptors (designer receptors exclusively activated by a designer drug) directly in the stroke area on week 13. Transfected neurons are silenced after i.p administration of the DREADD ligand, clozapine-N-oxide (CNO) on week 16.

Author Manuscript Author Manuscript Author Manuscript Author Manuscript

Mice are then submitted to the same behavioral tests: Cylinder (D1), Grid (D2), and Pasta (D3–D4).

Empty gel = HA hydrogel, Vs = 200 ng of soluble VEGF, lcV = 2μg nH loaded with 200 ng VEGF, hcV = 0.01 μg nH loaded with 200 ng VEGF and 0.99 μg unloaded nH. Data represent the average ± SEM (n = 12 mice) and p values were determined by One-way ANOVA, Tukey's post-hoc test, * indicating $P < 0.05$.

Author Manuscript Author Manuscript Author Manuscript Author Manuscript

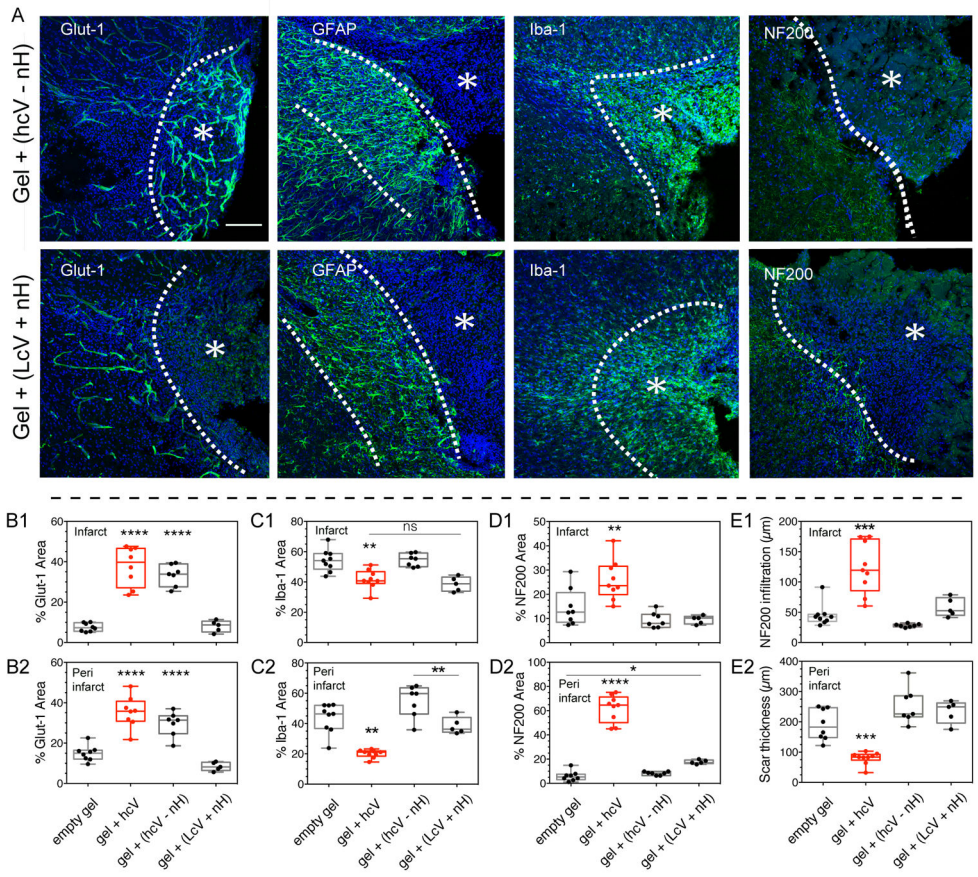

Figure 6. Role of naked heparin particles in the hcV treatment at 2 weeks post-stroke

Since the injected high and low cluster treatments (respectively hcV and lcV) were designed to contain equal amounts of heparin and VEGF, the VEGF clusterization in the hcV treatment was obtained on a low amount of heparin, leaving a high amount of naked particles. In order to understand the contribution of these naked particles in the pro-repair effect of the hcV, two supplemental group were studied: the hcV – nH where the naked particles from the hcV were removed, and the LcV + nH where additional naked particles were added to the low VEGF cluster condition. (A) Fluorescent images of vessels (Glut-1), astrocytic scar (GFAP), microglia (Iba-1) and axonal neurofilaments (NF200) in and around the stroke site (*) of gel + (hcV – nH) and LcV + nH) conditions, 2 weeks post-stroke. Quantitative assessment of the vascular area in the infarct (B1) and the peri-infarct area (B2), microglial area in the infarct (C1) and the peri-infarct area (C2), axonal area in the infarct (D1) and the peri-infarct area (D2), axonal infiltration distance (E1) and astrocytic scar (E2) at 2 weeks post-stroke.

hcV – nH = 0.01 μg nH loaded with 200 ng VEGF, lcV = 1μg nH loaded with 200 ng VEGF and 0.99 μg unloaded nH. Data is presented using a min to max box plot. Each dot in the plots represents one animal and p values were determined by One-way ANOVA with a Tukey's post-hoc test, with **, *** and **** indicating $p < 0.01$, $p < 0.001$ and $p < 0.0001$, respectively. Data represent the average. Scale bar: 100 μm.